Research Article

Bassam A. Mohammed*

Probing microstructural evolution and surface hardening of AISI D_3 steel after multistage heat treatment: An experimental and numerical analysis

https://doi.org/10.1515/jmbm-2025-0036
received July 24, 2024; accepted January 12, 2025

Abstract: In this study, different heat treatment cycles such as martempering, austempering, quenching, and quench tempering were applied to American Iron and Steel Institute (AISI) D_3 tool steel. Optical microscopy, scanning electron microscopy, and molecular dynamics (MD) approaches were utilized to evaluate the heat-treated microstructures. Moreover, the hardness and microhardness of the specimens were studied. The austempered specimen showed lower hardness than the partially and fully martempered specimens due to the formation of a bainitic matrix. On the other hand, the hardness loss of the fully martempered specimen was insignificant due to its low-carbon martensite matrix and alloy carbide hardness. Tempering of quenched specimens changed the carbide alloy from M_3C to M_3C_7, increasing the microhardness from 1,150 to 1,756 HV, whereas martensite microhardness decreased from 817 to 485 HV. The observed hardness reduction of the quench-tempered specimen suggests that the matrix part of an alloy significantly contributes to its hardness. The MD simulation results reveal that grain boundaries act as favorable sites for thermal twin formation in the microstructure during the tempering of the quenched specimen. A large concentration of such thermal twins would be another reason for the hardness loss of the tempered specimen.

Keywords: AISI D_3 steel, heat treatment, alloy carbides, hardness, molecular dynamics simulations

*** Corresponding author: Bassam A. Mohammed,** Thermal Mechanic Techniques Engineering Department, Basra Engineering Technical College, Southern Technical University, Basra, Iraq,
e-mail: bassam.moh@stu.edu.iq

1 Introduction

A major class of alloy steel with numerous industrial applications is categorized as tool steel. According to the AISI/SAE (American Iron and Steel Institute/Society of Automotive Engineers) standard, tool steel falls into seven main categories. Marked with specific letters, this classification is based on cooling methods after heat treatment, special applications, and primary features [1,2].

This tool steel is utilized in a variety of industrial applications due to its high hardness, excellent wear resistance, and dimensional stability. It is particularly suitable for making cutting dies, cold-forming dies, punching tools, and cutting blades in metal-forming processes. It is also used in producing parts that need to withstand severe wear conditions, such as wire drawing dies and precision tools. The high chromium content (about 12%) in the chemical composition of this steel ensures its relative resistance to corrosion, although it is not optimal for wet environments. The cold work tool steel is a prominent category of the tool steel class, falling into several subcategories. The cold work tool steel D category consists of 2–2.35% carbon and 11–13% chromium. This type of steel is employed to manufacture cutting tools and forming molds for operation at 260°C [3,4]. In this category, the steel is made up of M_3C and M_3C_7 carbides, which account for 18.5–23.5% of the volume percentage in quenched and austempered samples [5].

Different heat treatment methods, such as martempering, austempering, and quench-tempering, are used to achieve favorable microstructures and hardness [6]. Martempering treatment is a kind of modified quenching treatment for reducing residual stress and distortion caused by quenching [7]. Austempering is a kind of isothermal heat treatment that produces bainite structures in steel. This treatment is considered an alternative to quench-tempering treatment; however, it improves the flexibility

and impact resistance of steel in addition to reducing the chances of cracks caused by quenching. Requiring a specific salt bath, this treatment is also applied to a limited number of steels [6].

The sol–gel process has emerged as a highly effective method for enhancing the surface properties of cold-cutting tool steels, as noted in previous studies [8,9]. This technique enables the production of ceramic and nanocomposite coatings that exhibit exceptional resistance to wear, corrosion, and high temperatures. These coatings not only enhance the surface hardness of the steel but also serve as a protective barrier against damage from wear and challenging environmental conditions. Moreover, the coatings derived from the sol–gel process demonstrate superior corrosion resistance, which can substantially extend the service life of cold-cutting tools [10,11]. The ability of the sol–gel process to provide precise control over surface characteristics, such as roughness and adhesion, further contributes to the improved performance of industrial tools across various manufacturing and material-forming applications [12,13].

AISI D_3 tool steel, due to its specific chemical composition and resilient microstructure, is one of the most important materials for industrial applications requiring high hardness and wear resistance. The fatigue resistance of this steel under intermittent and severe loading conditions is particularly crucial, as it ensures the long-term performance of tools and dies. Selecting and optimizing the appropriate heat treatment can significantly enhance the fatigue resistance of this steel, thereby reducing repair and replacement costs [14–17].

Previous experimental investigations have shown that the presence of massive carbides plays one of the most critical roles in hardness and, therefore, can noticeably affect the mechanical behavior of such steels. In this context, Nykiel and Hryniewicz [5] analyzed the effects of carbides in these steels during the heat treatment at different temperatures. The results indicated that iron carbides (*e.g.*, Fe_3C) were observed within lower temperature ranges from 200 to 350°C, whereas chromium alloy carbides were observed from 500 to 700°C. They were completely insoluble in the austenite phase. In another study, Hariningsih *et al.* [18] compared the bainite and martensite microstructures of such steels at different austenitization temperatures. According to their results, the amount of carbon existing in the martensite phase was affected by the type of alloy carbide created in the microstructure. Samuel and Prabhu [19] observed that decreasing the tempering temperatures of these steels reduced their hardness.

Apart from the aforementioned carbides, a literature review reveals that the formation of thermal twins in the process of tempering high-carbon steels is an important factor that can change their mechanical properties [20–22]. Consequently, the D_3 tool steels are prone to these crystalline defects after heat treatment. Ehle *et al.* [23] analyzed the residual stress caused by the formation of thermal twins in a tempered AISI D_3 sample. Nevertheless, the experimental observations are quite scarce.

Molecular dynamics (MD) simulation methods allow researchers to study and predict the behavior of materials at the atomic level by simulating the interactions between atoms over time. This approach is particularly useful for investigating complex phenomena such as phase transitions, diffusion, and the mechanical properties of materials, as it provides detailed insights into atomic arrangements and movement. In contrast, finite element methods (FEMs) are typically used to analyze larger-scale structures and materials by dividing them into smaller, manageable elements. While FEM is effective for understanding macroscopic mechanical behavior and stress distribution, it does not provide the same level of detail regarding atomic interactions and microstructural changes. The advantage of using MD simulations lies in their ability to capture the dynamic processes occurring at the atomic scale, allowing for the exploration of time-dependent phenomena and the effects of temperature, pressure, and other environmental factors on material properties. This capability makes MD simulations an invaluable tool in materials science, enabling researchers to reduce experimental costs and time while gaining a deeper understanding of the fundamental mechanisms driving material behavior [24].

In recent years, MD simulation has increasingly been used as an efficient tool to analyze the effects of crystalline defects on the mechanical properties and microstructures of materials [25,26]. Karewar *et al.* [27] used this approach to study the effects of pre-existing twins on the phase transition process (from the austenite phase to the martensite phase). According to their observations, the twining boundaries were considered suitable sites for generating the martensite phase from the austenite phase. Samawi *et al.* reported that cracks would appear less often in a sample where the thermal twin was larger [28]. Therefore, the presence of twins while annealing can have direct effects on the mechanical properties of samples.

In the present study, we aim to understand the effects of tempered microstructures of the AISI D_3 tool steel on its hardness at different heat treatment protocols. For this purpose, different cycles of heat treatment were first applied to this steel, and the resultant values were compared through the hardness test. Moreover, scanning electron and optical microscopes (OM) were employed to scrutinize the annealed structures of samples, and the MD

Table 1: The chemical compound of the AISI D_3 steel with its equivalent in different standards [3]

%Fe	%W	%V	%Cr	%Si	%S	%P	%Mn	%C
Balance	0.03	0.25	12.2	0.30	0.01	0.01	0.12	2.12

Table 3: The properties of the etchant solution [7]

Name of the solution	Components
Vilella's reagent	1(g) picric acid + 5(ml) HCL + 100(ml) ethanol

simulation method was utilized to analyze the formation of thermal twins during the complete martempering treatment. Section 2 reports the details of samples, heat treatment protocols, and MD simulation. The results are discussed in Section 3, and the conclusion is drawn in Section 4.

2 Materials and methods

2.1 The experimental procedure

In this study, disc-shaped samples of a 5-cm thickness were made of the AISI D_3 (DIN: X 210 Cr 12) steel with a chemical compound shown in Table 1. The samples underwent different heat treatments (*i.e.*, quenching, quench-tempering, austempering, incomplete martempering, and complete martempering), the details of which can be seen in Table 2. The austempering treatment of samples lasted for 20 min at 930°C, and water was used as a cooling environment to quench the samples [29]. The cross-sections of all samples were scrutinized and recorded with a reflective OM [30]. In addition, a scanning electron microscope (SEM) was employed to analyze the microstructures of samples. After the polishing operation, the samples were exposed to an etchant solution with an appropriate mixture suitable for the steel. Table 3 presents the properties of the etchant solution. The hardness test was conducted with the Vickers indenter at 30 kg of load to compare samples in hardness. This test was repeated five times on each sample, and the mean result was reported. Furthermore, the micro-hardness test was conducted to compare different sections of microstructures (*e.g.*, alloy and matrix areas) in hardness.

2.2 Details of MD simulation

After examining and analyzing the SEM images, we employed MD simulations to further investigate the phases of the massive alloy carbides and to analyze stress concentration at the atomic scale. Given the limitations in analyzing twins at the atomic scale, this method allowed for a more accurate investigation of these microstructural defects. In this study, all simulations were performed on LAMMPS [31], which is an open-source software program. The atoms that account for less than 1% of the structure, as reported in Table 1, were disregarded to reduce the computational costs. Therefore, the representative elementary volume consisted of iron, chromium, and carbon atoms. The embedded atom method (EAM) potential function [32] was employed to define the interaction between the atoms of Fe and those of Cr in force and energy fields, whereas the EAM/alloy potential function was used to determine the Fe–C interaction and the Cr–C interaction. According to the literature, these potential functions can properly simulate the microstructures of carbon steels in a solid state [33]. According to Figure 1, a cubic sample with an edge length of 40 nm and an average grain size of 12 nm were used to analyze the effects of heat treatment on crystalline defects in the microstructure of the AISI D_3 tool steel. The orientation of grains in this sample was selected completely randomly. Before heat treatment, the sample was annealed with an isothermal-isobaric (NPT) ensemble and a

Table 2: The cycles of heat treatments applied to the AISI D_3 steel samples

Sample	Heat treatment cycle
As-received	
Austempered	Austenitization at 930°C for 20 min, rapid transfer to another furnace at 250°C, retention for 2 h, cooling in air
Partially martempered	Austenitization at 930°C for 20 min, rapid transfer to another furnace at 250°C, retention for 3 min, cooling in water
Fully martempered	Austenitization at 930°C for 20 min, rapid transfer to another furnace at 250°C, retention for 3 min, cooling in water, and tempering at 350°C for 1 h.
Quenched	Austenitization at 930°C for 20 min, rapid cooling in water
Quench-tempered	Austenitization at 930°C for 20 min, rapid cooling in water, and tempering at 350°C for 2 h.

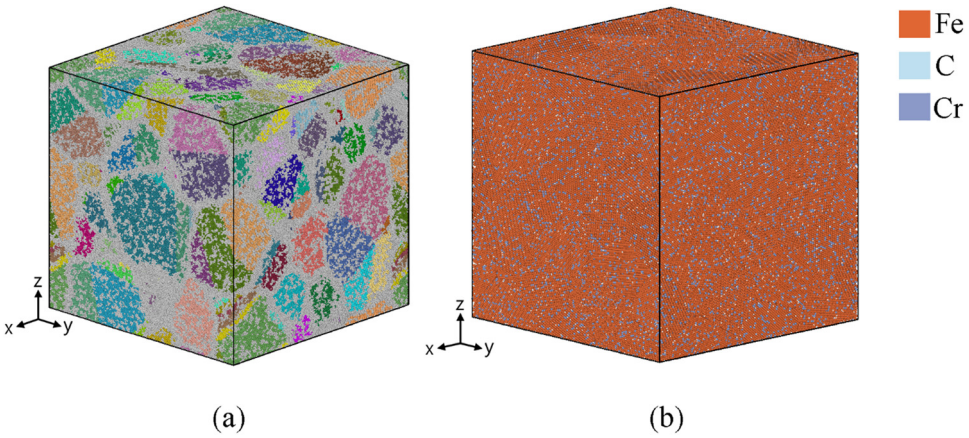

Figure 1: Polycrystalline configuration of D_3 steel sample with an average grain size of 10 nm. Atoms were colored based on: (a) grain segmentation analysis and (b) chemical composition.

Nosé–Hoover barostat at zero pressure and 300 K for 300 ps. Based on previous studies [34–36], such annealing process could successfully minimize the energy at grain boundaries. It is worth mentioning that the Maxwell–Boltzmann distribution was employed to determine the initial velocity of atoms and motion equations were solved through the velocity-Verlet algorithm to update the position and velocity of atoms [37]. In all three directions, the periodic boundary conditions were considered. The sample was first heated up from 300 to 1,203 K with a heating rate of 0.1 K/ps. It was kept at that temperature for 900 ps to simulate austempering treatment. For tempering, the sample was then annealed at 550 for 950 ps with a cooling rate of 0.1 K/ps. In this stage, the cooling rate was increased to simulate annealing in water; therefore, the sample was annealed from 550 to 300 K with a cooling rate of 10 K/ps for 25 ps. Finally, the sample was annealed at 650 K for 350 ps to perform the fully martempered treatment, and its annealed microstructure was studied with analysis tools in OVITO [38].

3 Results and discussion

3.1 Microstructure evolution of the tempered samples

Figure 2 shows a comparison drawn between the microstructures of the tempered samples with different protocols and those of the as-received sample using SEM results. As seen in this figure, massive and fine alloy carbides are formed in the microstructures of all tempered samples. According to previous studies [39–41], a large portion of the matrix austenite turns into martensite and bainite. Depending on the holding period at the desired temperature, the residual austenite then turns into bainite or ferrite. Figure 2 demonstrates the structure of the matrix for these samples as the tempered martensite. Furthermore, alloy carbides are formed when austenite is cools down, containing a kind of M_3C within 600–800°C and 5–25% of chromium [42]. The element represented by M can be either Fe or Cr. Figure 3 depicts massive chromium-based carbides in the fully martempered sample at different magnifications. As seen, when the D_3 steel is heated within the range of 380–600°C, a considerable percentage of its carbide is Cr_3C_7, and chromium makes up nearly 25–45% of the steel. In this context, most studies have revealed that the prominent role of these alloy carbides in enhancing the abrasion resistance and hardness of these steels. In this regard, Khun *et al.* [43] reported that the smaller dimensions of alloy carbides, a more normal distribution, and residual austenite were the key factors that increased the abrasion resistance of such steels. However, Song *et al.* [44] indicated that a normal distribution of fine carbides in the residual martensite in the austenite matrix would increase the hardness of such steels. In addition to the mentioned issues, the microstructure and morphology of such tool steels are under the influence of the thermal twin formation. Before heat treatment, the alloy carbides in the microstructure of the samples are fine and dispersed, limiting their effect on increasing hardness and microhardness. Therefore, the multi-stage heat treatment process transforms the martensite structure into a bainite structure, where massive alloy carbides with very high hardness form, significantly increasing the surface hardness of the samples. In conclusion, the multi-stage heat treatment changes the morphology of the alloy carbides from fine,

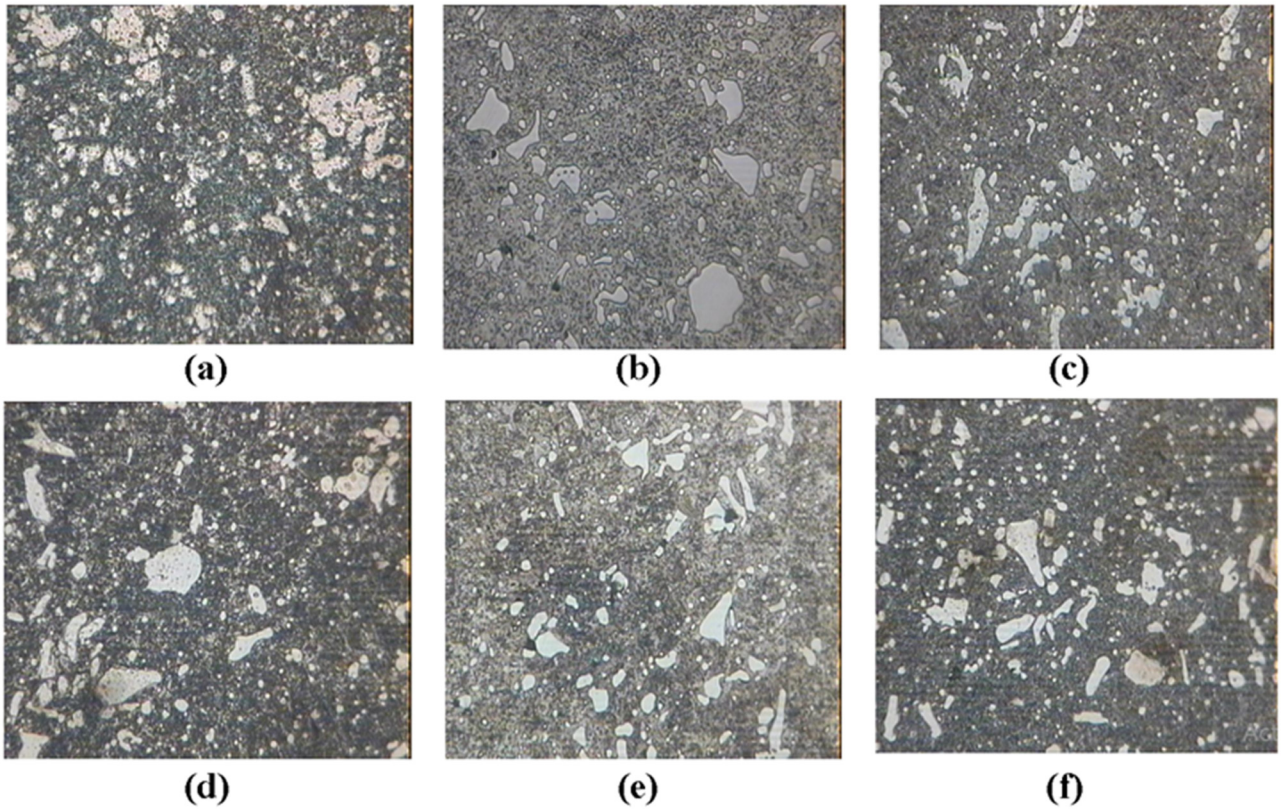

Figure 2: The OM images of the microstructure of tempered samples: (a) as-received, (b) quenched, (c) quench-tempered, (d) austempered, (e) fully martempered, and (f) partially martempered.

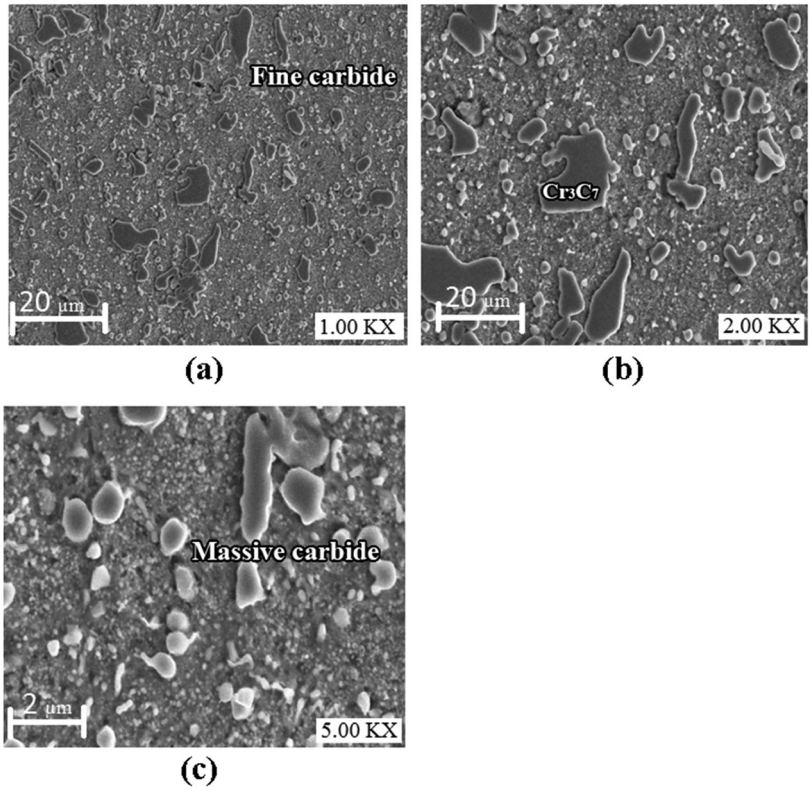

Figure 3: The SEM images of microstructures of the fully martempered sample at different magnifications: (a) fine carbides and (b and c) massive carbides.

agglomerated islands to massive alloy carbides with a more appropriate distribution.

In a recent study by Momeni *et al.* [39], it was observed that adding titanium and niobium while reducing chromium content can increase the secondary hardness of D_3 tool steel. However, the strength and toughness of these steels are reduced. Nykiel and Hryniewicz [5] observed the formation of thermal twins in the martensite matrix and even inside alloy carbides. Therefore, it was deduced that the mechanical properties of these steels are affected by alloy carbides and crystallite defects such as thermal twins.

In a study by Ehle *et al.* [23], a two-stage liquid nitrogen cooling and deep rolling process was designed for these steels to control the twinning and martensitic transformation phenomena after austenitizing heat treatment. The results show that the hardness of these steels can be increased from 355 HV0.1 to about 850 HV0.1.

As mentioned earlier, the presence of thermal twins caused by the annealing process can affect the mechanical properties of these steels.

A review of previous studies indicates that thermal twins forming in the structure of steels during heat treatment can be effectively observed using TEM microscopes [45,46]. However, the information obtained from these twins is typically limited to their crystal planes. In recent years, MD simulations have provided more comprehensive insights, such as the preferred locations of twin formation, the observation of twin boundaries, and the thickness of the twins. Since twins form at the atomic scale, MD simulations prove to be highly efficient for this analysis [47,48].

To shed more light on this issue, the thermal twin formation in the microstructure of the fully martempered sample has been atomistically probed through the MD simulation. According to Figure 4, these twins are seen in a large number of grains. In this figure, the green atoms indicate the crystalline structure of body-centered cubic, whereas the white atoms represent the positions of grain boundaries and carbide areas. Furthermore, the red atoms indicate the atomic layers existing in twin boundaries. It has been shown that such twins inside the grains can obstruct the slipping path of dislocations and improve mechanical properties by changing the crystalline orientation of grains [49,50]. According to Karewar *et al.* [27] study, thermal twins emerging in the austenite grains can become potential areas for the sprouting of the martensite phase from the austenite phase. Therefore, the presence of the thermal twins within the tempered microstructure of the samples would manifest itself in the change in the percentage of different phases.

As observed in Figure 4, the twins that nucleated from the grain boundary regions initiated growing inside the grains. Previous observations attribute the reason for this phenomenon to the high levels of energy in grain boundaries, which can reduce the activation energy barrier for the nucleation of these crystalline defects [51–54]. To shed more light on this issue, Figure 5 discloses the results of the von-Mises stress distribution analysis for the desired sample. The high values of stress in grain boundaries make these areas a favorite site for twin nucleation. Similarly, the alloy carbides are another prone site for twin formation due to their stress concentration. Consequently, it is expected that the high levels of stress at the carbides/martensite interface in the matrix would be a determining factor in the mechanical properties of such tool steels.

3.2 Surface hardness of tempered samples

Recent studies indicate that surface properties such as roughness, hardness, and morphology are very important for service conditions under load and surface modification

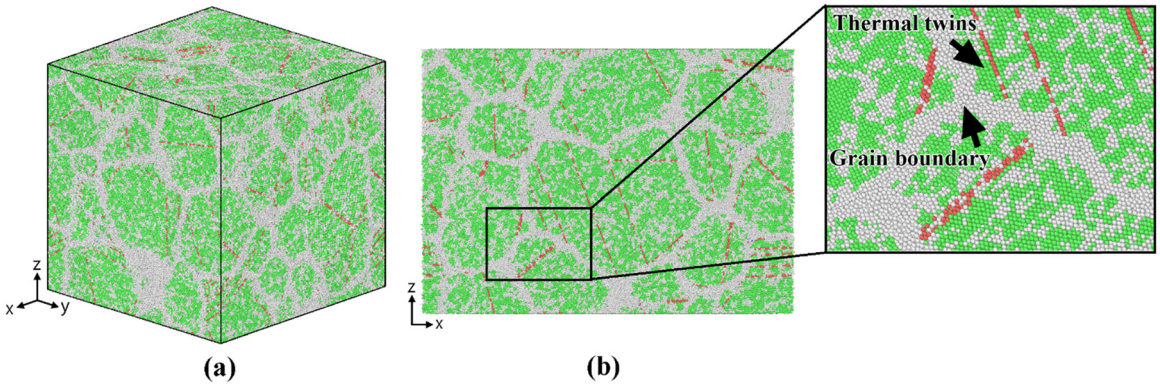

Figure 4: The Common Neighbor Analysis results for the fully martempered sample: (a) 3D view and (b) cross-section.

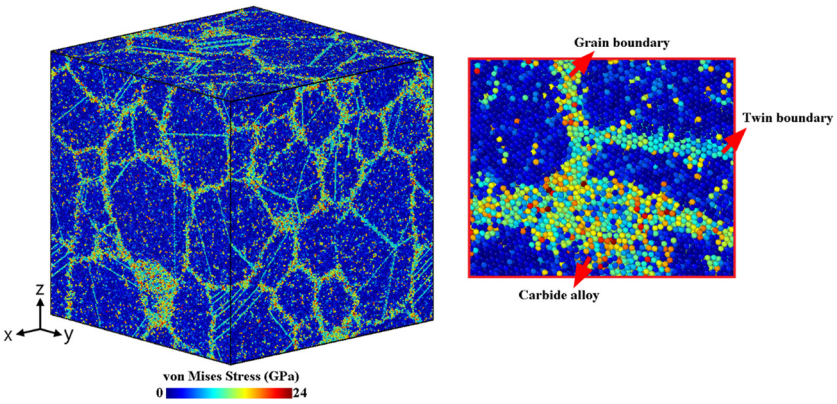

Figure 5: The von-Mises stress distribution map results for the fully martempered sample. Dark blue atoms show grain interiors and bright blue, yellow, orange, and red atoms represent highly stressed atoms.

(functionalization) operations. Based on these studies, methods that incorporate experimental tests, machine learning, and finite element models for these types of steels containing bulk alloy carbides provide optimal conditions for the thermal conductivity of cutting fluids and cutting temperatures to achieve better surface quality during the machining process [55–58]. A review of studies reveals that the surface hardness of these steels, in terms of microstructure after heat treatment, has been less investigated. The hardness test was conducted on all samples to establish a relationship between the microstructures of samples and their mechanical properties. Figure 6 displays the hardness test outcomes indicating that the hardness of the austempered sample is lower than that of the partially martempered sample. It arises because the austempered sample was tempered at 250°C for 1 h, during which there was enough time for the diffusion of carbon resulting in the transformation of the austenite phase into the bainite one. However, the martempered sample was placed at the foregoing temperature for merely 3 min; as a result, it still had a martensite matrix as discussed in Momeni *et al.* [39]. Since atomic diffusion is a time-consuming phenomenon, the martempered sample did not have enough time to change from a martensite matrix into a bainite one when it tempered at 250°C. Therefore, it still had a martensite structure.

According to previous studies, the partially martempered D_3 steels have residual stress and distortion due to their martensite matrix; therefore, they are not suitable for industrial use and need to undergo stress relieving using tempering treatments [59–61]. The formation of chromium carbides after heat treatment plays a crucial role in enhancing the hardness of AISI D_3 steel. These fine and hard carbides improve resistance to plastic deformation by

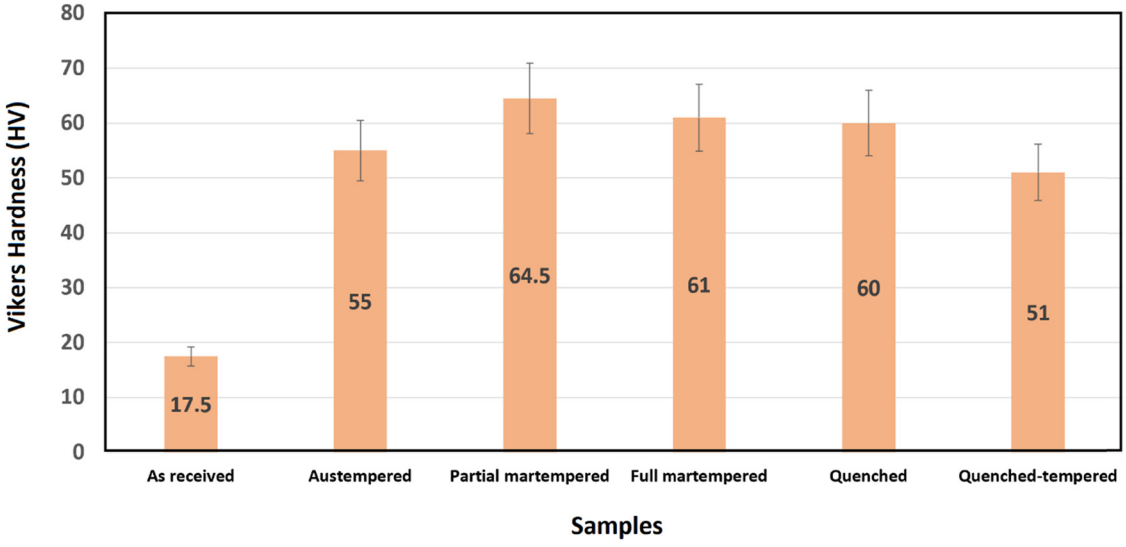

Figure 6: Measured hardness of the tempered samples.

creating obstacles to dislocation movement. Furthermore, their presence at grain boundaries prevents grain growth and strengthens grain boundaries. These effects, combined with the martensitic structure resulting from quenching, lead to a substantial increase in surface hardness and wear resistance, making the steel suitable for high-stress engineering applications. Regarding this issue, this sample was tempered at 350°C for 1 h, a treatment that was introduced as fully martempering in this study. It has been demonstrated that tempering such high-carbon tool steels is a time-consuming process [62,63]. Since there was no sufficient time for the diffusion of all carbon atoms, the low-carbon martensite structure emerged in the matrix. Therefore, the hardness of this sample is expected to remain nearly intact.

As seen in Figure 6, the fully martempered sample shows a minor reduction in hardness compared to the partially martempered counterpart. In other words, the presence of low-carbon martensite in the matrix of the fully martempered sample retained the high hardness of samples. Additionally, the role of carbides in the hardness should still be taken into account. In this regard, similar studies have indicated that the formation of iron carbides, *e.g.*, Fe_3C, can sharply increase the hardness of these steels [64].

Moving on to the next sample, the quenched one had a distribution of alloy carbides in the high-carbon martensite matrix. As viewed in Figure 6, the hardness of this sample is 60 RC. Given the residual stress in the microstructure of this sample, it must undergo stress relieving by further tempering treatments [4,65]. Therefore, this sample was placed at 350°C for 2 h. According to Figure 6, a significant hardness reduction was observed in the quench-tempered sample. This significant hardness reduction can be understood by the fact that the alloy carbides in the quenched sample were of the M_3C type, the hardness of which lies within the range of 1,060–1,240 Vickers with 25% chromium [5]. In the tempering treatment, these carbides turn into M_3C_7 carbides with 50% chromium whose hardness lies within the range of 1,500–1,800 Vickers [5]. As seen in Table 4, the measured hardness of all carbides existing in the quenched sample was 1,150 Vickers, whereas the hardness of carbides existing in the tempered sample was 1,756 Vickers. Nevertheless, since the tempering treatment was applied to the quenched sample for 2 h, the growth of carbides during the treatment increased the adsorption of carbon from the matrix, and the low-carbon martensite formed around carbides. Therefore, the matrix hardness in the tempered sample is expected to decline much more than that of the quenched sample [12]. According to the results of analyzing the matrix hardness in both samples, the matrix hardness of the quenched sample was twice that of the tempered sample. According to the hardness test results in Figure 6, the total hardness reduction indicates the greater role of matrix hardness than the carbide phase hardness in determining the total hardness.

Table 4: Measured microhardness of the quenched and quench-tempered samples

Sample	Microhardness of matrix (HV 0.2)	Microhardness of carbides (HV 0.2)
Quenched	817	1,150 ± 9.54
Quench-tempered	485	1,756 ± 10.12

According to the results obtained, the hardness of AISI D_3 steels is influenced by two main factors: matrix hardness and alloy carbide hardness. In the matrix, the quenching process creates a high density of dislocations in the martensitic structure due to the increased cooling rate, enhancing the hardness through the strain-hardening phenomenon. Since the martensite phase lacks softening mechanisms, its hardness remains very high. However, the residual stresses induced by the quenching process can reduce the mechanical strength of the steel, which can be addressed through multi-stage heat treatments. Regarding alloy carbides, these structures, which form at the grain boundaries, are very stable and possess high hardness due to the strong bond between chromium and carbon atoms. These carbides impede dislocation slip and enhance the stability of the grain boundaries, thereby reducing grain slip and increasing resistance to plastic deformation. Tempering and martempering heat treatments reduce the carbon in martensite and transfer it to alloy carbides, increasing carbide hardness. Although this process reduces the hardness of the matrix, the increase in the hardness of the alloy carbides compensates for this reduction, resulting in an overall insignificant decrease in sample hardness.

As expected, the hardness of the as-received sample is significantly lower than that of the other samples. The non-uniformity of the chemical composition and the presence of residual stress have contributed to a decrease in the plastic deformation resistance of this sample. The hardness of the austempered sample is lower than that of the other samples that underwent multi-stage heat treatment. This phenomenon can be attributed to the fact that, during the austempering process, the microstructure consists mainly of bainite rather than martensite. Bainite exhibits lower hardness than martensite due to its combination of ferrite and fine carbides, which reduces the density of dislocations and, consequently, the hardness of the matrix. Additionally, the residual stresses typically present in martensite, caused by quenching, are either eliminated or reduced in the

bainite microstructure. This further contributes to the overall decrease in sample hardness. Although the bainite microstructure possesses higher deformation resistance and toughness, its hardness is generally lower than that of martensitic microstructures. As previously discussed, the formation of martensite in samples cooled in a water environment after austenitization increases the matrix hardness. However, due to the high residual stress, the martempering heat treatment reduces the carbon content in the matrix martensite, transferring it to the alloy carbide phase. This results in decreased matrix hardness and increased hardness of the carbide phase, leading to minimal overall change in the hardness of the entire sample.

4 Conclusion

In this study, experimental observations and MD simulations were employed to analyze the microstructure and hardness of the AISI D_3 tool steel tempered at different heat treatment protocols. The results indicated that annealing the partially martempered samples reduced their stress, changed the matrix microstructure to low-carbon martensite, and slightly decreased hardness. Moreover, when the quenched sample was tempered, the chemical compound of carbides changed from M_3C to M_3C_7, increasing the hardness of the carbides. Therefore, the significant reduction of the total hardness is caused by the reduction in matrix hardness. Overall, if high hardness and structural stability are considered important parameters, full martempering is the best heat treatment to produce a component with no residual stress while maintaining high hardness and having a normal distribution of alloy carbides in this type of tool steel. Full martempering denotes austenitization at 930°C for 20 min, rapid transfer to another furnace at 250°C, retention for 3 min, cooling in water, and tempering at 350°C for 1 h. In the case of the fully martemped sample, MD simulation outcomes showed that thermal twins nucleated from grain boundaries and emitted within a large number of grains. This phenomenon was attributed to the high concentration of stress in grain boundaries. Since twin boundaries are prone to the formation of martensite from austenite, their high density reduced the residual austenite in the sample microstructure.

Acknowledgments: The author extends their appreciation to Southern Technical University, Basra, Iraq, for supporting this work.

Funding information: Author states no funding involved.

Author contributions: The author has accepted responsibility for the entire content of this manuscript and approved its submission.

Conflict of interest: Author states no conflict of interest.

Data availability statement: The datasets generated during and/or analyzed during the current study are available from the corresponding author on reasonable request.

References

[1] Roberts GA, Kennedy R, Krauss G. Tool steels. Ohio, US: ASM International; 1998.
[2] Avishan B, Karimkhani Shamloo R, Akbarzadeh Chiniforoush E, Yazdani S. Ultrafine carbide-free bainite in high-carbon steel after continuous annealing with different cooling rates. J Mater Eng Perform. 2023 Jun;32(11):4922–31.
[3] Totten GE. Steel heat treatment handbook-2 volume set. Florida, US: CRC Press; 2006.
[4] Yadav S, Dileep K, Jinoop AN, Paul CP, Rai AK, Singh R, et al. Laser directed energy deposition of high-carbon high-chromium D2 tool steel structures: processing, heat treatment and material behavior. J Mater Eng Perform. 2023 Jun;32(11):4881–91.
[5] Nykiel T, Hryniewicz T. Transformations of carbides during tempering of D3 tool steel. J Mater Eng Perform. 2014;23(6):2050–4.
[6] ASM Handbook Committee. Properties and selection: irons, steels, and high-performance alloys. Ohio, US: ASM International; 1990.
[7] Unterweiser PM, Boyer HE, Kubbs JJ. Heat treater's guide: standard practices and procedures for steel. Ohio: ASM International; 1982.
[8] Keziz A, Heraiz M, Sahnoune F, Rasheed M. Characterization and mechanisms of the phase's formation evolution in sol-gel derived mullite/cordierite composite. Ceram Int. 2023 Oct;49(20):32989–3003.
[9] Assoudi N, Chaabani A, Rasheed M, Walha I, Dhahri E, Alawsi T, et al. Comparative examination of the physical parameters of the sol gel produced compounds La0. 5Ag0. 1Ca0. 4MnO_3 and La0. 6Ca0. 3Ag0. 1MnO_3. Opt Quantum Electron. 2022 Sep;54(9):556.
[10] Keziz A, Rasheed M, Heraiz M, Sahnoune F, Latif A. Structural, morphological, dielectric properties, impedance spectroscopy and electrical modulus of sintered $Al_6Si_2O_{13}$–$Mg_2Al_4Si_5O_{18}$ composite for electronic applications. Ceram Int. 2023 Dec;49(23):37423–34.
[11] Sellam M, Rasheed M, Azizii S, Saidani T. Improving photocatalytic performance: Creation and assessment of nanostructured SnO2 thin films, pure and with nickel doping, using spray pyrolysis. Ceram Int. 2024 Jun;50(12):20917–35.
[12] Bouras D, Rasheed M. Comparison between CrZO and AlZO thin layers and the effect of doping on the lattice properties of zinc oxide. Opt Quantum Electron. 2022 Dec;54(12):824.
[13] Al-Darraji MN, Abdalkareem Jasim S, Aldeen OD, Ghasemian A, Rasheed M. The effect of LL37 antimicrobial peptide on FOXE1 and lncRNA PTCSC 2 genes expression in colorectal cancer (CRC) and normal cells. Asian Pac J Cancer Prev. 2022 Oct;23(10):3437.

[14] Wang H, Liu X, Chen T, Xu S. Prediction and evaluation of fatigue life via modified energy method considering surface processing. Int J Damage Mech. 2022 Mar;31(3):426–43.
[15] Wang J, Liu J, Hua F, He Y, Wang X. Critical plane-based fatigue life model under multiaxial random loading. Int J Struct Integr. 2022 Aug;13(5):845–56.
[16] Wang H, Liu X, Wu Q, Wang X, Wang Y. An improved fatigue life prediction model for shock absorber cylinder with surface roughness correction. Eng Comput. 2021 Jul;38(6):2713–32.
[17] Lai J, Wang Y, Wei Y, Liang J, Liu X. The prediction of residual life of liquid-storage tank considering the tank wall surface state. Int J Struct Integr. 2022 Nov;13(6):985–98.
[18] Hariningsih H, Lutiyatmi L, Daryanto T. Effects of heat treatment on microstructure and hardness of D2 tools. Appl Res Smart Technol. 2022 Aug;3(1):29–37.
[19] Samuel A, Prabhu KN. Residual stress and distortion during quench hardening of steels: a review. J Mater Eng Perform. 2022 Jul;31(7):5161–88.
[20] Khan R, Pervez T, Qamar SZ, Alrasheedi NH, Al Abri O. Twinning and transformation induced plasticity in advanced steels: A thermodynamic modeling approach. In: Hashmi, editor. Comprehensive materials processing. 2nd edn. Oxford: Elsevier; 2024. p. 159–174.
[21] Ogawa Y. Temperature-sensitive ductilization in hydrogen-alloyed Fe-Cr-Ni austenitic steel by enhanced deformation twinning. Scr Mater. 2024 Jan;238:115760.
[22] Nie Y, Chang YT, Charpagne MA. Origins of twin boundaries in additive manufactured stainless steels. Acta Mater. 2024 May;275:120035.
[23] Ehle LC, Spille J, Meyer H, Kämmler J, Werner J, Schwedt A, et al. Controlled twinning and martensitic transformation in metastable AISI D3 (X210Cr12) steel by sequential deep rolling and liquid nitrogen cooling. Mater Today Commun. 2021 Sep;28:102484.
[24] Jaber AS, Ismael M, Rashid T, Sarhan MA, Rasheed M, Sala IM. Comparesion the electrical parameters of photovoltaic cell using numerical methods. EUREKA: Phys Eng. 2023 Jul;27(4):29–39.
[25] Mohammed BA, Batbooti RS. MD-based study on the deformation process of engineered Ni–Al core–shell nanowires: Toward an understanding underlying deformation mechanisms. Curved Layer Struct. 2023 Feb;10(1):20220188.
[26] Alshalal I, Al-Zuhairi HM, Abtan AA, Rasheed M, Asmail MK. Characterization of wear and fatigue behavior of aluminum piston alloy using alumina nanoparticles. J Mech Behav Mater. 2023 Apr;32(1):20220280.
[27] Karewar S, Sietsma J, Santofimia MJ. Effect of pre-existing defects in the parent fcc phase on atomistic mechanisms during the martensitic transformation in pure Fe: A molecular dynamics study. Acta Mater. 2018;142:71–81.
[28] Samawi KA, Mohammed BA, Salman EA, Mahmoud HM, Sameen AZ, Mohealdeen SM, et al. Vertical growth of a 3D Ni–Co-LDH/N-doped graphene aerogel: a cost-effective and high-performance sulfur host for Li–S batteries. Phys Chem Chem Phys. 2024;26(12):9284–94.
[29] Kara F, Küçük Y, Özbek O, Özbek NA, Gök MS, Altaş E, et al. Effect of cryogenic treatment on wear behavior of Sleipner cold work tool steel. Tribol Int. 2023 Feb;180:108301.
[30] Kadri E, Dhahri K, Barillé R, Rasheed M. Novel method for the determination of the optical conductivity and dielectric constant of SiGe thin films using Kato-Adachi dispersion model. Phase Transit. 2021 Feb;94(2):65–76.
[31] Plimpton S. Fast parallel algorithms for short-range molecular dynamics. J Comput Phys. 1995 Mar;117(1):1–9.
[32] Daramola A, Bonny G, Adjanor G, Domain C, Monnet G, Fraczkiewicz A. Development of a plasticity-oriented interatomic potential for CrFeMnNi high entropy alloys. Comput Mater Sci. 2022 Feb;203:111165.
[33] Bonny G, Bakaev A, Terentyev D. The combined effect of carbon and chromium enrichment on < 1 0 0 > loop absorption in iron. Comput Mater Sci. 2022 Aug;211:111533.
[34] Mustafa MA, Abdullah AR, Hasan WK, Habeeb LJ, Nassar MF. Two-way fluid-structure interaction study of twisted tape insert in a circular tube having integral fins with nanofluid. East-Eur J Enterp Technol. 2021 Jun;3(8):111.
[35] Kardani A, Mehrafrooz B, Montazeri A. MD-based computational design of new engineered Ni-based nanocatalysts: An in-depth study of the underlying mechanism. Eur Phys J Plus. 2018 Mar;133:1–9.
[36] Kardani A, Montazeri A, Urbassek HM. Strain-rate-dependent plasticity of Ta-Cu nanocomposites for therapeutic implants. Sci Rep. 2023 Sep;13(1):15788.
[37] Allen MP, Tildesley DJ. Computer simulation of liquids. Oxford, UK: Oxford University Press; 2017.
[38] Stukowski A. Visualization and analysis of atomistic simulation data with OVITO–the Open Visualization Tool. Model Simul Mater Sci Eng. 2009 Dec;18(1):015012.
[39] Momeni M, Kheirandish S, Saghafian H, Hedjazi J, Momeni M. Effects of heat treatment on mechanical properties of modified cast AISI D3 tool steel. Mater Des (1980-2015). 2014 Feb;54:742–7.
[40] Mathews JA, Sietsma J, Petrov RH, Santofimia MJ. Austenite formation from a steel microstructure containing martensite/austenite and bainite bands. J Mater Res Technol. 2023 Jul;25:5325–39.
[41] Lu X, Yang Z, Qian D, Lan J, Hua L. Effect of martensite pre-quenching on bainite transformation kinetics, martensite/bainite duplex microstructures, mechanical properties and retained austenite stability of GCr15 bearing steel. J Mater Res Technol. 2021 Nov;15:2429–38.
[42] Kheirandish S, Saghafian H, Hedjazi J, Momeni M. Effect of heat treatment on microstructure of modified cast AISI D3 cold work tool steel. J Iron Steel Res Int. 2010 Sep;17(9):40–5.
[43] Khun NW, Liu E, Tan AWY, Senthilkumar D, Albert B, Mohan Lal D. Effects of deep cryogenic treatment on mechanical and tribological properties of AISI D3 tool steel. Friction. 2015;3(3):234–42.
[44] Song RG, Zhang K, Chen GN. Electron beam surface treatment. Part I: surface hardening of AISI D3 tool steel. Vacuum. 2003;69(4):513–6.
[45] Kim JK. In-situ TEM investigation of deformation mechanisms of twinning-induced plasticity steel. Mater Charact. 2023 Feb;196:112583.
[46] Wittig JE, Pierce DT, Mosecker L, Saeed-Akbari A, Beigmohamadi M, Mayer J. TEM investigation of deformation mechanisms in FeMnCrCN TWIP steel. Microsc Microanal. 2013 Aug;19(S2):1736–7.
[47] Zhou XW, Wadley HN. Twin formation during the atomic deposition of copper. Acta Mater. 1999 Feb;47(3):1063–78.
[48] Kardani A, Montazeri A. Metal-matrix nanocomposites under compressive loading: Towards an understanding of how twinning formation can enhance their plastic deformation. Sci Rep. 2020 Jun;10(1):9745.
[49] Pourboghrat F, Park T, Kim H, Mohammed B, Esmaeilpour R, Hector LG. An integrated computational materials engineering approach for constitutive modelling of 3rd generation advanced

high strength steels. In Journal of Physics: Conference Series. Vol. 1063. Issue 1. IOP Publishing; 2018 Jul 1. p. 012010.
[50] Alshaeer F, Zorah M, Mahmoud HM, Abdalgadir LM, Taki AG, Mohammed BA, et al. Bandgap-engineered MXene-g-C3N4 interfacial layer for enhanced charge carrier dynamics in perovskite solar cells. J Alloy Compd. 2024 Dec;1011:178247.
[51] Karewar S, Hidalgo J, Sietsma J, Santofimia MJ. Role of planar faults in martensite formation in nano-polycrystalline iron by molecular dynamics simulation. J Mater Sci. 2022 Oct;57(37):17678–99.
[52] Galindo-Nava EI, Rivera-Díaz-del-Castillo PE. Understanding martensite and twin formation in austenitic steels: A model describing TRIP and TWIP effects. Acta Mater. 2017 Apr;128:120–34.
[53] Kardani A, Montazeri A, Urbassek HM. Unraveling the temperature-dependent plastic deformation mechanisms of polycrystalline Ta implants through numerical analysis of grain boundary dynamics. J Mater Sci. 2022 Sep;57(34):16490–506.
[54] Kardani A, Montazeri A, Urbassek HM. Computational analysis of the mechanical properties of Ta/Cu nanocomposite dental implants: On the role of incoherent interfaces. Met Mater Int. 2023 Aug;29(8):2385–97.
[55] Gemechu LD, Efa DA, Abebe R. Optimizing CNC turning of AISI D3 tool steel using Al_2O_3/graphene nanofluid and machine learning algorithms. Heliyon. 2024 Dec;10(24):e40969.
[56] Shinge VR, Pable MJ. Effect of nano-minimum quantity lubrication on cutting temperature and surface roughness of milling AISI D_3 tool steel. Mater Today: Proc. 2023 Jan;72:1758–64.
[57] Azami A, Salahshournejad Z, Shakouri E, Sharifi AR, Saraeian P. Influence of nano-minimum quantity lubrication with MoS_2 and CuO nanoparticles on cutting forces and surface roughness during grinding of AISI D2 steel. J Manuf Process. 2023 Feb;87:209–20.
[58] Bangarraju B, Chinamilli NS, Prasanna V, Bhanuprakash C. Development and solving of optimization model for WEDM of AISI D3 using TLBO algorithm. Mater Today: Proc. 2023 Jun, in Press.
[59] Gavriljuk VG, Theisen W, Sirosh VV, Polshin EV, Kortmann A, Mogilny GS, et al. Low-temperature martensitic transformation in tool steels in relation to their deep cryogenic treatment. Acta Mater. 2013 Mar;61(5):1705–15.
[60] Karakaş MS. Tribocorrosion behavior of surface-modified AISI D_2 steel. Surf Coat Technol. 2020 Jul;394:125884.
[61] Dwivedi AP, Choudhury SK. Estimation of recast layer thickness in rotary tool EDM process for machining AISI D3 tool steel. Mater Today: Proc. 2017 Jan;4(10):10816–22.
[62] Lipchin NN, Sten'kin PA. Austempering of carbon steels from high temperatures. Met Sci Heat Treat Met. 1959 May;1:65–6.
[63] Prasetyo MA, Sofyan N, Ridlo FM, Mabruri E. Effect of tempering temperature on mechanical and corrosion properties of modified martensitic stainless steel CA6NM. Met Sci Heat Treat. 2024 Jan;65(9):657–62.
[64] Kaba M, Filiz HI, Cui Z, Baydogan M, Cimenoglu H, Alpas AT. Microstructural effects on impact-sliding wear mechanisms in D_2 steels: The roles of matrix hardness and carbide characteristics. Wear. 2024 Feb;538:205224.
[65] Wang J, Li H, Wang Q, Liang Z, Gao S, Sun L, et al. Effect of rapid tempering at high temperature on microstructure, mechanical properties and stability of retained austenite of medium carbon ultrafine bainitic steel. J Mater Res Technol. 2024 Jan;28:3144–54.